Light-scattering technique for the study of dynamic thickness fluctuations in thin liquid films

Richard C. Haskell, Daniel C. Petersen, and Mark W. Johnson*
Physics Department, Harvey Mudd College, Claremont, California 91711
(Received 14 September 1992)

We describe a light-scattering technique capable of probing the dynamics of thickness fluctuations in lipid bilayers. The technique, which we call reflectance fluctuation spectroscopy (RFS), is keenly sensitive to light scattered from the squeeze modes of motion in a thin liquid film, and insensitive to light scattered from the bend modes. A laser beam is focused to a small spot on the film, and the power in the specularly reflected beam is recorded in real time. Thickness fluctuations associated with the squeeze modes of motion give rise to fluctuations in the power of the specularly reflected light. The frequency spectrum of the fluctuations in detected power (RFS spectrum) can be analyzed to yield values for the film viscosity and thickness compressibility. We present two independent theoretical derivations of the RFS spectrum and show that scattering from the bend mode can be neglected. The theoretical expression for the RFS spectrum is compared with experimental spectra obtained from glycerylmonooleate–decane bilayers. The fit of the theory to the data is excellent and the values deduced for the film viscosity and thickness compressibility are reasonable.

PACS number(s): 68.15.+e, 87.22.Bt

I. INTRODUCTION

A thin liquid film, surrounded on both sides by a fluid medium, exhibits two collective modes of motion which are excited by the random thermal motion of the constituent molecules. The squeeze mode, also called the peristaltic mode, involves thickness fluctuations (see Fig. 1) whose dynamic behavior is determined by the thickness compressibility, interfacial tension, and viscosity of the film. Thickness fluctuations in lipid bilayers were first discussed we believe by Hladky and Gruen [1], and their existence has recently been inferred from time-averaged x-ray- and neutron-scattering data by Wiener and White [2]. The dynamics of collective motion in lipid bilayers have been studied by neutron scattering [3] and NMR [4], but these researchers could not determine whether the observed motion was associated with squeeze modes or with the bend modes to be discussed below. The effect of thickness fluctuations on the opening and closing of protein channels in lipid membranes has been studied by several groups of researchers [5–7]. In soap films, thickness fluctuations have been studied by dynamic light scattering (DLS) as a means of probing the electrostatic double-layer repulsive force and the Van der Waals attractive force [8–10].

The second collective mode of a thin liquid film is the bend mode, also called the undulation mode, which maintains constant film thickness (see Fig. 1). Its dynamic behavior is determined primarily by the interfacial tension and the viscosity of the surrounding fluid. The bend mode in lipid bilayers was first observed by Grabowski and Cowen [11] using dynamic light scattering, and extensive DLS measurements were performed subsequently by Crilly and Earnshaw [12]. By performing DLS measurements of bend modes, Crawford and Earnshaw [13] monitored values of lipid bilayer tension, and determined the temperature of a chain-melting phase transition. In soap films, the bend mode has been observed by Joosten and Fijnaut [14], Young and Clark [10], and Joosten [15] using DLS.

The roughness of a lipid bilayer on the spatial scale of a protein channel (a few nanometers) is due to approximately equal contributions from squeeze and bend modes. Yet, on the scale of the wavelength of light, the amplitude of bend motion far exceeds that of the squeeze modes. Hence, while sufficient light is scattered by bend modes to make possible DLS studies of bend-mode dynamics, very little light is scattered by squeeze modes, leading Crawford and Earnshaw [16] to describe the squeeze modes as "essentially unobservable" in lipid bilayers. One notable exception is the report by Miyakawa, Hirakawa, and Yamashita [17] of squeeze modes in a bilayer of oxidized cholesterol and tetradecane. Their novel DLS geometry employed a bilayer in the shape of a spherical bubble.

We are interested primarily in the effect of thickness fluctuations on the opening and closing of protein chan-

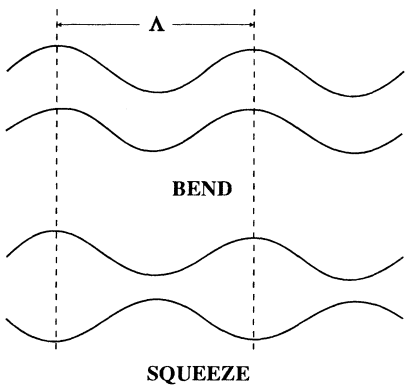

FIG. 1. The normal modes of motion of a thin liquid film.

nels. Accordingly, we have designed a light-scattering technique with enhanced sensitivity to squeeze modes and greatly reduced sensitivity to bend modes. The technique is remarkably simple, and we shall refer to it as reflectance fluctuation spectroscopy (RFS). A laser beam is focused to a small spot (a few micrometers) on a membrane, and the intensity of the specularly reflected light is recorded. Squeeze modes with wavelengths longer than the diameter of the beam spot make the membrane appear to the incident beam as a roughly planar film with a time-varying thickness. These thickness fluctuations lead to fluctuations ($\approx 0.1\%$) in the intensity of the specular reflection, and analysis of the frequency spectrum of these intensity fluctuations (the RFS spectrum) yields values for the film viscosity and thickness compressibility.

RFS is insensitive to bend motion for two reasons. First, bend modes with wavelengths that are long compared to the beam diameter simply result in translational motion of the film toward and away from the incident beam. While this translational motion leads to Doppler phase shifts in the reflected electric field, the reflected intensity is unaffected. Bend modes (and squeeze modes) with wavelengths shorter than the illuminated spot on the film scatter light at angles too high to be included in the specularly reflected beam. The second reason that RFS is insensitive to bend motion is that the dynamic time scale of squeeze modes is many orders of magnitude slower than that of bend modes. As a result, the frequency spectrum of fluctuations in the reflected intensity due to squeeze modes is concentrated in a frequency interval much narrower than that of the bend modes, so the amplitude of the squeeze spectrum is much greater than that of the bend spectrum.

The purpose of this paper is to describe in detail our RFS light-scattering technique. We present two theoretical approaches—one involving the macroscopic theory of thin-film interference, and the second a molecular light-scattering approach in which RFS is described as a variation of dynamic light scattering. We compare our theoretical expressions for the RFS spectrum with experimental spectra obtained from glyceryl monooleate (GMO)–decane bilayers. The agreement is striking and the values deduced for the membrane viscosity and thickness compressibility are reasonable. A complete discussion of our bilayer results will be presented in a subsequent paper.

Most of the present paper is devoted to theoretical derivations of the RFS spectrum. In Sec. II, we begin by describing the dynamics of squeeze and bend modes, providing a review of the results of hydrodynamic theory applied to thin liquid films [18,19]. In Sec. III, we derive the RFS spectrum by employing the macroscopic theory of thin-film interference. While this is a simple, intuitive approach, it cannot be used to describe light scattering from bend motion. Hence, in Sec. IV, we resort to a molecular theory of light scattering which can describe scattering from both squeeze and bend modes. RFS emerges as a variation of dynamic light scattering in which the fluctuating field scattered from a squeeze or bend mode is heterodyned with the constant specularly reflected field. In Sec. V, experimental RFS spectra obtained from GMO–decane bilayers are presented and compared with theory.

II. FILM HYDRODYNAMICS

Lucassen *et al.* [18], Vrij *et al.* [19], and Joosten [20,21] have studied the hydrodynamics of a thin liquid film bounded on both sides by semi-infinite fluid media. All media in this film system are assumed to be incompressible, isotropic, and homogeneous, and the linearized Navier-Stokes equation is used to describe the motion of a fluid element. Boundary conditions are imposed at the two surfaces of the film: the fluid velocity is required to be continuous across each interface, as are the normal and tangential components of the stress tensor. Our primary interest is in so-called "symmetric" film systems, in which the film is surrounded by the same fluid medium on both sides.

For symmetric films, two normal modes emerge from the equations of motion (see Fig. 1). The bend mode is a propagating wave that maintains constant film thickness; the restoring force is provided by interfacial tension. The squeeze mode is nonpropagating for most films of interest and exhibits thickness fluctuations. The restoring force for the squeeze mode is provided by interfacial tension and by the thickness compressibility U''—the second derivative with respect to thickness of the free energy per unit area of the film. It is important to keep in mind that the film is modeled as an incompressible fluid, so that no changes in film density occur in the theory. Rather, the thickness "compressibility" U'' is a measure of the restoring force opposing changes in thickness of the film. In the case of lipid bilayers, U'' is provided primarily by the steric and entropic repulsive forces between hydrocarbon chains. The squeeze disturbance depicted in Fig. 1 is restored to a planar film by the movement of fluid from a thick region of the film to a thin region.

The equations of motion plus boundary conditions yield a dispersion equation for the squeeze mode [Eq. (4) of [19]]. For squeeze wavelengths Λ of interest, the dispersion equation predicts frequencies that are purely imaginary, $\omega = i\Gamma$, so that squeeze modes are excited thermally and relax exponentially in time. An approximate analytical expression for the relaxation rate is given by Vrij *et al.* [19]:

$$\Gamma = \frac{h_0^3 K^2}{12\eta}\left[U'' + \frac{\sigma K^2}{2}\right], \tag{2.1}$$

where h_0 is the average hydrodynamic thickness of the film, η is the film viscosity, σ is the interfacial tension (film tension $\approx 2\sigma$), and $K = 2\pi/\Lambda$ is the squeeze wave number. We have found that this expression for Γ is within 0.5% of the exact numerical solution to the dispersion equation for a GMO–decane bilayer in the wavelength range $1\ \mu\text{m} < \Lambda < 1$ mm, which is the relevant range for our light-scattering measurements.

The dispersion equation for the bend mode [Eq. (36) of [18]] yields nonzero real and imaginary parts of the frequency, $\omega = \omega_{\text{bend}} + i\Gamma_{\text{bend}}$, for bend wavelengths and films

of interest. Joosten [21] has suggested very approximate analytical expressions for the real frequency and the relaxation rate:

$$\omega_{\text{bend}}=\frac{\left[\frac{2\sigma}{\rho h_0}\right]^{1/2}K}{\left[1+\frac{3\rho'}{\rho h_0 K}\right]^{1/2}},$$
$$\Gamma_{\text{bend}}=\left[\frac{1+\frac{4\eta'}{\eta h_0 K}}{1+\frac{3\rho'}{\rho h_0 K}}\right]\frac{\eta}{2\rho}K^2, \tag{2.2}$$

where ρ,η and ρ',η' are the densities and viscosities of the film and surrounding medium, respectively. In the wavelength range $1\ \mu\text{m}<\Lambda<1$ mm, these expressions can be a factor of 3 different from the exact numerical solution to the dispersion equation for a GMO–decane bilayer. For light-scattering calculations involving the bend mode of this bilayer, we have used the somewhat more accurate empirical relations

$$\omega_{\text{bend}}=2.05\times10^{-3}K^{1.48},\quad \Gamma_{\text{bend}}=1.11\times10^{-5}K^{1.8}. \tag{2.3}$$

To gain an appreciation for the sensitivity of our light-scattering technique, we compare the amplitudes of thermally generated squeeze and bend motions. The mean-square thickness fluctuation due to squeeze modes with wave numbers between $K_{\min}$ and $K_{\max}$ can be shown to be [1,9]

$$\langle(\Delta h)^2\rangle=\frac{k_BT}{2\pi\sigma}\ln\left[\frac{K_{\max}^2+\frac{2U''}{\sigma}}{K_{\min}^2+\frac{2U''}{\sigma}}\right], \tag{2.4}$$

and similarly the mean-square film displacement due to bend modes is

$$\langle d^2\rangle=\frac{k_BT}{4\pi\sigma}\ln\left[\frac{K_{\max}}{K_{\min}}\right]. \tag{2.5}$$

Table I lists the root-mean-square amplitudes for a GMO–decane bilayer. Notice that for disturbances experienced by a macromolecule ($\Lambda\geq10$ nm), the amplitudes of the two types of motion are comparable, but for disturbances probed by visible light ($\Lambda\geq1\ \mu$m), the bend displacements are roughly 20 times larger than the thickness fluctuations. Our light-scattering technique is designed to be insensitive to film displacements so that the smaller thickness fluctuations can be detected.

III. LIGHT-SCATTERING THEORY: THIN-FILM INTERFERENCE

A useful, intuitive description of our RFS light-scattering technique can be gained by employing the standard theory of thin-film interference. When the wavelength of a squeeze mode is much longer than the diameter of the illuminated spot, the incident beam experiences the film as an effectively planar film with a time-varying thickness. These fluctuations in thickness then produce fluctuations in the power of the reflected beam. When the wavelength of a squeeze mode is comparable to or shorter than the diameter of the illuminated beam, we shall assume that each differential area of the beam is reflected according to the local thickness of the illuminated differential area of the film. The total reflected power can then be calculated by integrating over the total illuminated area [see Eq. (3.1)]. In the integration, thickness fluctuations with wavelengths shorter than the beam diameter present an average thickness to the beam and do not contribute to fluctuations in the reflected power. We have found that this macroscopic approach leads to predictions essentially identical to those of the more fundamental microscopic calculations presented in Sec. IV.

When a Gaussian spherical beam is incident normally on a thin film with a local instantaneous optical thickness $h_{\text{op}}(x,y,t)$, the reflected power is given by [23]

$$P_{\text{reflected}}(t)=\int\int dx\,dy\,I_{\text{incident}}(x,y)\times4\frac{(n-1)^2}{(n+1)^2}\sin^2[k_2h_{\text{op}}(x,y,t)], \tag{3.1}$$

where the intensity profile of the incident beam is

$$I_{\text{incident}}(x,y)=P_0\frac{2}{\pi w_f}\exp\left[-\frac{2(x^2+y^2)}{w_f^2}\right] \tag{3.2}$$

and P_0 is the power in the incident beam. The radius (containing 86% of the beam power) of the illuminated spot on the film is w_f, and the integral in Eq. (3.1) is over the illuminated film. The refractive index of the film is n_2, that of the surrounding medium is n_1, and their ratio is defined as $n=n_2/n_1$. The wave number of light in the film is $k_2=2\pi n_2/\lambda_0$ where λ_0 is the wavelength in vacuum. In Eq. (3.1), we have assumed that the Fresnel reflection coefficient $(n-1)^2/(n+1)^2$ associated with each interface is small. For a water-oil interface, this reflection coefficient is approximately 0.1%.

TABLE I. Amplitudes of thermally generated motion in a GMO–decane bilayer. We have used an interfacial tension of $\sigma=3.84$ mN/m [22] and a thickness compressibility of $U''=10^{13}$ J/m^4.

Normal mode	Range of Λ	rms amplitude (nm)
Thickness fluctuations (Δh)	1 μm–1 mm	0.036
due to squeeze modes	10 nm–1 mm	0.86
Film displacement (d)	1 μm–1 mm	0.76
due to bend modes	10 nm–1 mm	0.99

Fluctuations in the local thickness of the film, $\Delta h(x,y,t)$, give rise to fluctuations in the reflected power:

$$\Delta P_{\text{reflected}}(t)=\int\int dx\,dy\, I_{\text{incident}}(x,y) \times 4\frac{(n-1)^2}{(n+1)^2}2\sin(k_2 h_{\text{op}}) \times\cos(k_2 h_{\text{op}})k_2\Delta h(x,y,t)\ , \quad (3.3)$$

where h_{op} is the time-averaged optical thickness at every point on the film, and we have kept only the leading term in a Taylor series expansion about h_{op}. We can write the thickness fluctuations as a Fourier sum over all squeeze modes:

$$\Delta h(x,y,t)=\sum_{\mathbf{K}}\Delta h(\mathbf{K},t)\exp(i\mathbf{K}\cdot\mathbf{r}_f)\ , \quad (3.4)$$

where the squeeze wave number is defined by $K=2\pi/\Lambda$ (see Fig. 1). Then the mean-square fluctuation in reflected power can be written

$$\langle[\Delta P_{\text{reflected}}(t)]^2\rangle=\left[P_0 8\frac{(n-1)^2}{(n+1)^2}k_2\sin(k_2 h_{\text{op}}) \times\cos(k_2 h_{\text{op}})\right]^2 \times\sum_{\mathbf{K}}\langle|\Delta h(\mathbf{K},t)|^2\rangle\exp(-\tfrac{1}{4}w_f^2K^2)\ , \quad (3.5)$$

where we have used the statistical independence of thermally generated squeeze modes,

$$\langle\Delta h^*(\mathbf{K},t)\Delta h(\mathbf{K}',t)\rangle=\delta_{\mathbf{K},\mathbf{K}'}\langle|\Delta h(\mathbf{K},t)|^2\rangle\ ,$$
$$\langle\Delta h(\mathbf{K},t)\Delta h(\mathbf{K}',t)\rangle=\delta_{\mathbf{K},-\mathbf{K}'}\langle|\Delta h(\mathbf{K},t)|^2\rangle\ . \quad (3.6)$$

The sum over squeeze wave vectors in Eq. (3.5) can be converted to an integral over wave number according to

$$\sum_{\mathbf{K}}\rightarrow\left[\frac{L}{2\pi}\right]^2\int_0^\infty 2\pi K\,dK\ , \quad (3.7)$$

where the film size is taken to be $L\times L$. The mean-square-thickness fluctuation associated with a thermally generated squeeze mode with wave number K has been calculated by Vrij, Joosten, and Fijnaut [9]:

$$\langle|\Delta h(\mathbf{K},t)|^2\rangle=\frac{1}{L^2}\frac{2k_BT}{\sigma K^2+2U''}\ , \quad (3.8)$$

where σ is the interfacial tension and U'' is the second derivative with respect to thickness of the free energy per unit area of film. As mentioned in Sec. II, a squeeze disturbance does not propagate but simply relaxes exponentially in time with a decay rate Γ given by Eq. (2.1). The frequency spectrum of thickness fluctuations associated with a squeeze mode with wave number K is therefore a Lorentzian function centered at zero frequency with a half width at half maximum of $\Gamma(K)$ (rad/sec):

$$\langle|\Delta h(\mathbf{K},t)|^2\rangle=\langle|\Delta h(\mathbf{K},t)|^2\rangle \times 4\int_0^\infty d\nu\frac{\Gamma(K)}{(2\pi\nu)^2+[\Gamma(K)]^2}\ , \quad (3.9)$$

where ν is the frequency in Hz. With these substitutions, Eq. (3.5) becomes

$$\langle[\Delta P_{\text{reflected}}(t)]^2\rangle=\left[P_0 8\frac{(n-1)^2}{(n+1)^2}k_2\sin(k_2 h_{\text{op}})\cos(k_2 h_{\text{op}})\right]^2 \times\int_0^\infty\frac{K\,dK}{2\pi}\frac{2k_BT}{\sigma K^2+2U''}\exp(-\tfrac{1}{4}w_f^2K^2)4\int_0^\infty d\nu\frac{\Gamma(K)}{(2\pi\nu)^2+[\Gamma(K)]^2}\ . \quad (3.10)$$

Experimentally we find it convenient to measure the frequency spectrum of fluctuations in the detected power normalized by the square of the average power, where the average power is given approximately by

$$\langle P_{\text{reflected}}\rangle\cong P_0 4\frac{(n-1)^2}{(n+1)^2}\sin^2(k_2 h_{\text{op}})\ . \quad (3.11)$$

If we define the normalized spectrum of the detected power, $S(\nu)$, in terms of the normalized mean-square fluctuations in reflected intensity,

$$\frac{\langle[P_{\text{reflected}}-\langle P_{\text{reflected}}\rangle]^2\rangle}{\langle P_{\text{reflected}}\rangle^2}\equiv\int_0^\infty d\nu S(\nu)\ , \quad (3.12)$$

we have finally for $S(\nu)$:

$$S(\nu)=\frac{k_BT}{\pi}16k_2^2\frac{\cos^2(k_2 h_{\text{op}})}{\sin^2(k_2 h_{\text{op}})}\int_0^\infty\frac{K\,dK}{\sigma K^2+2U''}\exp(-\tfrac{1}{4}w_f^2K^2)\frac{\Gamma(K)}{(2\pi\nu)^2+[\Gamma(K)]^2} \quad (3.13)$$

where $\Gamma(K)$ is given by Eq. (2.1). Notice that $S(\nu)$ is a weighted sum of Lorentzians, and, as a result, has the general shape of a Lorentzian centered at zero frequency.

The expression above for $S(\nu)$, the spectrum of intensity fluctuations due to squeeze modes, has been derived with a simple extension of the theory of thin-film interference. Yet the result, Eq. (3.13), is essentially identical to the expression we will derive in Sec. IV using a more involved microscopic theory of dynamic light scattering. We include the treatment in Sec. IV because it is easily extended to describe scattering from the bend modes. We see no simple extension of the methods of the present sec-

tion that is capable of showing rigorously that our measured spectra are due predominantly to thickness fluctuations and not to motion associated with bend modes.

IV. LIGHT-SCATTERING THEORY: DYNAMIC LIGHT SCATTERING

Our RFS light-scattering technique can be viewed as an application of dynamic light scattering [24] in which the fluctuating scattered field is heterodyned with the constant, specularly reflected field. In this section, we develop a microscopic description of RFS based upon a heterodyne DLS approach. This microscopic theory is capable of describing light scattering from both squeeze and bend modes in a thin liquid film.

Consider a Gaussian spherical beam incident normally on a thin liquid film in the x-y plane. The film has refractive index n_2 and the index of the surrounding liquid is n_1. Figure 2 depicts the film perturbed by the presence of a squeeze mode with wave vector $\mathbf{K}=\hat{\mathbf{y}}2\pi/\Lambda$, where Λ is the wavelength of the disturbance. The incident electric field propagating in the surrounding medium is given by

$$\mathbf{E}_{\text{incident}}(\mathbf{r},t)=\hat{\mathbf{x}}A_0\left[\frac{2}{\pi}\right]^{1/2}\frac{1}{w}\exp(i\Psi)\times\exp\{-i[k_1(z-z_0)+\omega t]\}\times\exp\left[-i\frac{k_1}{2}\frac{x^2+y^2}{\tilde{r}}\right], \tag{4.1}$$

where $\Psi=\arctan[(z-z_0)/z_R]$ and the Rayleigh range is $z_R=\pi w_0^2/\lambda_1$ [25]. The complex radius of curvature is given by $\tilde{r}=z-z_0+iz_R$ [25] and $k_1=2\pi/\lambda_1$, where λ_1 is the wavelength of light in the surrounding medium. The beam radius (86%) is given by $w=w_0\{1+[(z-z_0)/z_R]^2\}^{1/2}$, where the waist radius $w_0=3.25$ μm in our experimental setup. According to Eq. (4.1), the waist is located in the plane $z=z_0$ and the radius of the illuminated spot on the film (at $z=0$) is

$$w_f=w_0\left[1+\left[\frac{z_0}{z_R}\right]^2\right]^{1/2}. \tag{4.2}$$

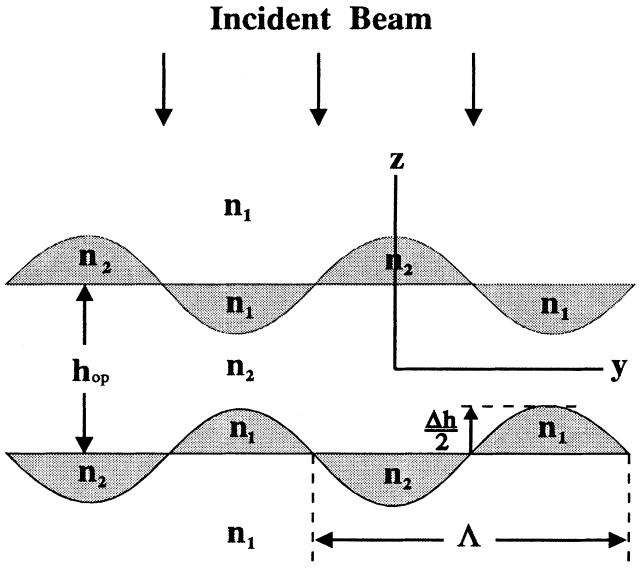

FIG. 2. A thin liquid film perturbed by a squeeze mode of wave number $K=2\pi/\Lambda$.

A. Scattered electric field

The electric field scattered by the film in Fig. 2 can be conceptually divided into two components: (1) the field $\mathbf{E}_{\text{specular}}$ specularly reflected from a film with perfectly plane surfaces and uniform optical thickness h_{op}, and (2) the field $\mathbf{E}^{(\mathbf{K})}_{\text{squeeze}}$ scattered from the two sinusoidal interfacial layers (shaded), which impart to the film a squeeze mode of wave vector $\mathbf{K}$. This superposition of component fields follows naturally if the total oscillating *excess* polarization vector in the film is expressed as the superposition of (1) the excess polarization vector induced in a film with perfectly plane surfaces and uniform thickness h_{op}, and (2) the excess polarization vectors associated with the sinusoidal interfacial layers

$$\Delta\mathbf{P}_{\text{total}}(\mathbf{r},t)=\Delta\mathbf{P}_{\text{planar}}(\mathbf{r},t)+\Delta\mathbf{P}_{\text{top}}(\mathbf{r},t)+\Delta\mathbf{P}_{\text{bottom}}(\mathbf{r},t)\ . \tag{4.3}$$

We shall evaluate the component polarization vectors in Eq. (4.3) and then calculate the fields they radiate, $\mathbf{E}_{\text{specular}}$ and $\mathbf{E}^{(\mathbf{K})}_{\text{squeeze}}$.

First we note that at a position $\mathbf{r}$ in the material of a perfectly planar film, the excess polarization vector is (in SI units)

$$\Delta\mathbf{P}_{\text{planar}}(\mathbf{r},t)=(\chi_2-\chi_1)\epsilon_0\mathbf{E}_{\text{planar}}(\mathbf{r},t)\ , \tag{4.4}$$

where χ_2 and χ_1 are the electric susceptibilities of the film and surrounding medium, respectively. At a position $\mathbf{r}$ in the top sinusoidal interfacial layer, the excess polarization vector assumes one of two values,

$$\Delta\mathbf{P}_{\text{top}}(\mathbf{r},t)=\pm(\chi_2-\chi_1)\epsilon_0\mathbf{E}_{\text{top}}(\mathbf{r},t)\ , \tag{4.5}$$

where the plus (minus) sign holds when the position vector $\mathbf{r}$ lies in the top (bottom) half of the top sinusoidal interfacial layer. A similar relation holds for the bottom sinusoidal interfacial layer:

$$\Delta\mathbf{P}_{\text{bottom}}(\mathbf{r},t)=\mp(\chi_2-\chi_1)\epsilon_0\mathbf{E}_{\text{bottom}}(\mathbf{r},t)\ , \tag{4.6}$$

where the minus (plus) sign is associated with the top (bottom) half of the bottom sinusoidal interfacial layer.

If we confine our attention to very thin films ($\cong 5$ nm), the field reflected from a perfectly planar film will be small compared to the incident field. Then the boundary condition requiring continuity of the electric field allows us to approximate the field inside the planar film with $\mathbf{E}_{\text{planar}}\cong\mathbf{E}_{\text{incident}}$. In addition, if we assume that the perturbation of the squeeze mode does not alter the electric field in the material of the film but simply redistributes the material, we can approximate all the fields in Eqs. (4.4)–(4.6) by $\mathbf{E}_{\text{incident}}$.

As a check on Eqs. (4.3)–(4.6), we note that they yield the sensible result that any point $\mathbf{r}$ in the material of the film in Fig. 2,

$$\Delta \mathbf{P}_{\text{total}}(\mathbf{r},t)=(\chi_2-\chi_1)\varepsilon_0\mathbf{E}_{\text{incident}}(\mathbf{r},t)\ , \tag{4.7}$$

and at any point $\mathbf{r}$ in the surrounding medium $\Delta\mathbf{P}_{\text{total}}(\mathbf{r},t)$ is zero.

The radiation from the oscillating excess polarization vector associated with the perfectly planar film produces the specularly reflected field $\mathbf{E}_{\text{specular}}$. If the waist of the incident beam is formed on the film ($z_0=0$), then the incident wave front is planar and the standard application of boundary conditions to the electromagnetic field [23] yields the following form for the specularly reflected field:

$$\mathbf{E}_{\text{specular}}(\mathbf{r},t)=\hat{\mathbf{x}}2\frac{n-1}{n+1}\sin(k_2h_{\text{op}})\exp\left[i\left[k_2h_{\text{op}}+\frac{\pi}{2}\right]\right]$$
$$\times A_0\left[\frac{2}{\pi}\right]^{1/2}\frac{1}{w'(z_0=0)}\exp(-i\Psi_0')\exp[i(k_1z-\omega t)]\exp\left[i\frac{k_1}{2}\frac{x^2+y^2}{\tilde{r}_0'}\right]\ , \tag{4.8a}$$

where

$$n=\frac{n_2}{n_1}\ ,\quad k_2=\frac{2\pi}{\lambda_2}\ ,\quad \Psi_0'=\arctan(z/z_R)\ ,\quad w'(z_0=0)=w_0[1+(z/z_R)^2]^{1/2}\ ,$$

and $\tilde{r}_0'=z-iz_R$. In constructing Eq. (4.8a), we have assumed that the Fresnel reflection coefficient for the medium-film interface is small, and we have let $z\rightarrow -z$ in Eq. (4.1) to reverse the direction of propagation.

When the wave front of the incident beam is spherical ($z_0\neq 0$), the application of boundary conditions to the electromagnetic field becomes more complicated. Using the light-scattering approach that we will employ to calculate $\mathbf{E}^{(\mathbf{K})}_{\text{squeeze}}$, we have found that an additional phase term must be added to Eq. (4.8a):

$$\mathbf{E}_{\text{specular}}(\mathbf{r},t)=\hat{\mathbf{x}}2\frac{n-1}{n+1}\sin(k_2h_{\text{op}})\exp\left[i\left[k_2h_{\text{op}}+\frac{\pi}{2}\right]\right]$$
$$\times A_0\left[\frac{2}{\pi}\right]^{1/2}\frac{1}{w'}\exp(-i\Psi')\exp\{i[k_1(z+z_0)-\omega t]\}\exp\left[i\frac{k_1}{2}\frac{x^2+y^2}{\tilde{r}'}\right]\exp\left[-i\frac{x^2+y^2}{w'^2}\frac{z_0}{z_R}\right]\ , \tag{4.8b}$$

where

$$\Psi'=\arctan[(z+z_0)/z_R]\ ,\quad \tilde{r}'=z+z_0-iz_R\ ,\quad \text{and}\quad w'=w_0\{1+[(z+z_0)/z_R]^2\}^{1/2}\ .$$

The last term in Eq. (4.8b) depends upon the position of the beam waist, and an appreciation of this term and an analogous term in the expression for $\mathbf{E}^{(\mathbf{K})}_{\text{squeeze}}$ will prove critical for a full understanding of our experimental technique.

The field $\mathbf{E}^{(\mathbf{K})}_{\text{squeeze}}$ is generated by the oscillating excess polarization vectors associated with the interfacial layers. Let us calculate the dipole moments per unit area contained in the interfacial layers. The thicknesses a_{top} and a_{bottom} of the layers are equal to the displacements of the top and bottom interfaces from their averages positions at $z=+h_{\text{op}}/2$ and $z=-h_{\text{op}}/2$, respectively:

$$a_{\text{top}}(\mathbf{r}_f,t)=+\frac{\Delta h(\mathbf{K},t)}{2}\exp(i\mathbf{K}\cdot\mathbf{r}_f)\ ,$$
$$a_{\text{bottom}}(\mathbf{r}_f,t)=-\frac{\Delta h(\mathbf{K},t)}{2}\exp(i\mathbf{K}\cdot\mathbf{r}_f)\ , \tag{4.9}$$

where $\mathbf{r}_f=x\hat{\mathbf{x}}+y\hat{\mathbf{y}}$ is the position vector in the plane of the film, and the real parts of Eq. (4.9) correspond to physically observable quantities. Note that the fluctuation in thickness of the film associated with the squeeze mode can be written

$$\Delta h(\mathbf{r}_f,t)=h(\mathbf{r}_f,t)-h_{\text{op}}$$
$$=a_{\text{top}}(\mathbf{r}_f,t)-a_{\text{bottom}}(\mathbf{r}_f,t)$$
$$=\Delta h(\mathbf{K},t)\exp(i\mathbf{K}\cdot\mathbf{r}_f)\ . \tag{4.10}$$

For lipid bilayers, the thickness a_{top} or a_{bottom} of a thermally generated interfacial layer is much less than the wavelength of light, and the oscillating dipoles contained within a particular layer emit radiation fields with no appreciable phase difference due to their different positions in the z direction. Consequently, the excess polarization of the two interfacial layers can be modeled as two excess *surface* dipoles, $\mathbf{\Pi}_{\text{top}}$ and $\mathbf{\Pi}_{\text{bottom}}$ (dipole moment per unit area), located at $z=+h_{\text{op}}/2$ and $z=-h_{\text{op}}/2$:

$$\mathbf{\Pi}_{\text{top}}\left[\mathbf{r}_f,z=+\frac{h_{\text{op}}}{2},t\right]=a_{\text{top}}(\mathbf{r}_f,t)\Delta\mathbf{P}_{\text{top}}(\mathbf{r},t)$$
$$=(n^2-1)\epsilon_1\frac{\Delta h(\mathbf{K},t)}{2}\exp(i\mathbf{K}\cdot\mathbf{r}_f)\mathbf{E}_{\text{incident}}\left[\mathbf{r}_f,z=+\frac{h_{\text{op}}}{2},t\right]\ , \tag{4.11}$$

$$\Pi_{\text{bottom}}\left[\mathbf{r}_f, z=-\frac{h_{\text{op}}}{2}, t\right]=a_{\text{bottom}}(\mathbf{r}_f,t)\Delta\mathbf{P}_{\text{bottom}}(\mathbf{r},t)$$
$$=(n^2-1)\epsilon_1\frac{\Delta h(\mathbf{K},t)}{2}\exp(i\mathbf{K}\cdot\mathbf{r}_f)\mathbf{E}_{\text{incident}}\left[\mathbf{r}_f, z=-\frac{h_{\text{op}}}{2}, t\right] . \quad (4.12)$$

In constructing Eqs. (4.11) and (4.12), we have used Eqs. (4.5), (4.6), and (4.9), replacing the electric fields in Eqs. (4.5) and (4.6) with the incident field, and using the identity $(\chi_2-\chi_1)\epsilon_0=(n^2-1)\epsilon_1$, where ϵ_1 is the permittivity of the surrounding medium. Note that the signs in Eqs. (4.5), (4.6), and (4.9) are conveniently accounted for by the factor $\exp(i\mathbf{K}\cdot\mathbf{r}_f)$ in Eqs. (4.11) and (4.12).

These two excess surface dipoles can be combined into a single *effective* surface dipole radiating from the plane $z=0$ if the phases of the component surface dipoles are corrected for their respective z positions:

$$\Pi(\mathbf{r}_f, z=0, t)=(n^2-1)\epsilon_1\frac{\Delta h(\mathbf{K},t)}{2}\exp(i\mathbf{K}\cdot\mathbf{r}_f)\exp(-ik_1h_{\text{op}})\mathbf{E}_{\text{incident}}(\mathbf{r}_f, z=0, t)$$
$$+(n^2-1)\epsilon_1\frac{\Delta h(\mathbf{K},t)}{2}\exp(i\mathbf{K}\cdot\mathbf{r}_f)\exp(-ik_1h_{\text{op}}+i2k_2h_{\text{op}})\mathbf{E}_{\text{incident}}(\mathbf{r}_f, z=0, t)$$
$$=(n^2-1)\epsilon_1\Delta h(\mathbf{K},t)\exp(i\mathbf{K}\cdot\mathbf{r}_f)\exp[i(k_2-k_1)h_{\text{op}}]\cos k_2h_{\text{op}}\mathbf{E}_{\text{incident}}(\mathbf{r}_f, z=0, t) . \quad (4.13)$$

Each surface element $dx\,dy$ of this effective surface dipole constitutes an excess oscillating electric dipole $\Delta\mathbf{p}(\mathbf{r}_f, z=0, t)=\Pi(\mathbf{r}_f, z=0, t)dx\,dy$, which contributes to the scattered field at a distant detector an amount

$$\Delta\mathbf{E}^{(\mathbf{K})}_{\text{squeeze}}=\frac{1}{4\pi\epsilon_1R\left[\frac{c}{n_1}\right]^2}\left[\frac{\partial^2\Delta\mathbf{p}}{\partial t^2}\right]_{\text{retarded}} , \quad (4.14)$$

where R is the distance from the dipole to the point on the detector [26]. The second derivative of the dipole with respect to time is evaluated at the retarded time $t-R/(c/n_1)$.

With the help of Fig. 3, the distance R to the detector can be approximated by

$$R\cong R_0-\hat{\mathbf{k}}_s\cdot\mathbf{r}_f+\frac{x^2+y^2}{2R_0} , \quad (4.15)$$

where we introduce the scattered wave vector $\mathbf{k}_s$ and (for later) the incident wave vector $\mathbf{k}_i$ and the scattering vector $\mathbf{q}=\mathbf{k}_s-\mathbf{k}_i$,

$$\mathbf{k}_s=\frac{2\pi}{\lambda_1}\begin{bmatrix}\sin\theta\cos\phi\\ \sin\theta\sin\phi\\ \cos\theta\end{bmatrix} ,$$
$$\mathbf{k}_i=\frac{2\pi}{\lambda_1}\begin{bmatrix}0\\ 0\\ -1\end{bmatrix} , \quad (4.16)$$
$$\mathbf{q}=\frac{2\pi}{\lambda_1}\begin{bmatrix}\sin\theta\cos\phi\\ \sin\theta\sin\phi\\ 1+\cos\theta\end{bmatrix} .$$

The distance R can be replaced simply with R_0 in the denominator of Eq. (4.14), but the full form of the approximation in Eq. (4.15) must be used for the retarded time in the phase of Eq. (4.14).

The field $\mathbf{E}^{(\mathbf{K})}_{\text{squeeze}}$ scattered from the two interfacial layers in Fig. 2 can now be calculated by integrating Eq. (4.14) over the illuminated area of the film. Collecting Eqs. (4.1) and (4.13)–(4.16) and simplifying expressions,

$$\mathbf{E}^{(\mathbf{K})}_{\text{squeeze}}=-\frac{k_1^2(n^2-1)}{4\pi}\frac{\exp[i(k_1R_0-\omega t)]}{R_0}\Delta h(\mathbf{K},t)\exp[i(k_2-k_1)h_{\text{op}}]\cos k_2h_{\text{op}}$$
$$\times\hat{\mathbf{x}}A_0\left[\frac{2}{\pi}\right]^{1/2}\frac{1}{w_f}\exp(ik_1z_0)\exp(i\Psi_f)$$
$$\times\int\int dx\,dy\exp[i(\mathbf{K}-\mathbf{q})\cdot\mathbf{r}_f]\exp\left[-i\frac{k_1}{2}\frac{x^2+y^2}{\bar{r}_f}\right]\exp\left[i\frac{k_1}{2}\frac{x^2+y^2}{R_0}\right] , \quad (4.17)$$

where $\Psi_f=\arctan(-z_0/z_R)$ and $\bar{r}_f=-z_0+iz_R$. The integral can be performed by completing the squares in the exponent; we have finally

$$\mathbf{E}^{(\mathbf{K})}_{\text{squeeze}}=-\hat{\mathbf{x}}A_0\frac{k_1^2(n^2-1)w_0}{2\sqrt{2\pi}}\Delta h(\mathbf{K},t)\exp[i(k_2-k_1)h_{\text{op}}]\cos k_2h_{\text{op}}$$
$$\times\frac{\exp[i(k_1R_0-\omega t)]}{R_0}\exp(ik_1z_0)\exp\left[-\frac{w_0^2}{4}(\mathbf{K}-\mathbf{q}_f)^2\right]\exp\left[-i\frac{w_0^2}{4}(\mathbf{K}-\mathbf{q}_f)^2\frac{z_0}{z_R}\right] , \quad (4.18)$$

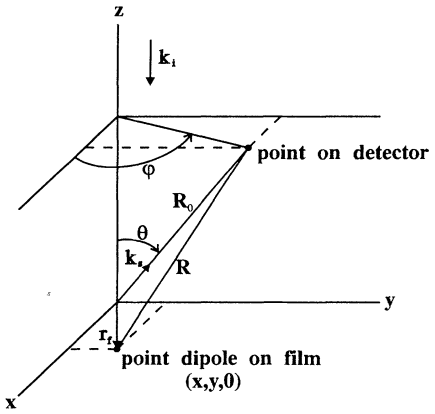

FIG. 3. Scattering geometry: R is the distance from an oscillating dipole on the film to a point on the detector.

where the projection of the scattering vector onto the film is $\mathbf{q}_f = q_x\hat{\mathbf{x}} + q_y\hat{\mathbf{y}}$.

The last phase factor in Eq. (4.18) is a noteworthy consequence of forming the waist a distance z_0 before the film. In our experimental setup, we vary z_0 to vary the size of the illuminated spot on the film according to Eq. (4.2). This last phase factor in Eq. (4.18) is similar to the last term in the expression for $\mathbf{E}_{\text{specular}}$ in Eq. (4.8b). Indeed, the term in Eq. (4.8b) can be evaluated at the position of the detector,

$$\exp\left[-i\frac{x^2+y^2}{w'^2}\frac{z_0}{z_R}\right] = \exp\left[-i\frac{w_0^2 q_f^2}{4}\frac{z_0}{z_R}\right].$$

Except for these phase factors, Eqs. (4.8b) and (4.18) have the standard form of a Gaussian spherical wave.

The intensity scattered by a squeeze mode alone is the absolute value squared of Eq. (4.18), so the last term involving z_0 drops out. This expression for the intensity has precisely the form of a Gaussian spherical wave with maximum intensity along the direction $\theta_{\max} = K/k_1 = \lambda_1/\Lambda$. In addition, the divergence half angle of the scattered beam is $\theta_{1/2} = \lambda_1/\pi w_0$, the same as that of the specular reflection given by the absolute value squared of Eq. (4.8b). These results indicate that the squeeze mode scatters light like a sinusoidal grating with spacing Λ.

It is important to emphasize that the electric field incident upon the detector in our experimental setup is never solely the field scattered by squeeze modes. In fact, the detector subtends a solid angle that includes the specularly reflected field and any scattered fields overlapping with the specular reflection. Hence, the detected intensity is never simply the absolute value squared of Eq. (4.18). When $w_0 \gg \Lambda$, i.e., when the incident beam illuminates many wavelengths of the squeeze mode even when the waist lies on the film ($z_0 = 0$), then $\theta_{\max} \gg \theta_{1/2}$, and there is no overlap between the beam scattered by the squeeze mode and the specular reflection. Therefore squeeze modes with $\Lambda \ll w_0$ never contribute to the intensity detected in our experimental setup.

However, when $w_0 < \Lambda$ and hence $\theta_{\max} < \theta_{1/2}$, the field scattered by the squeeze mode overlaps with the specular reflection, and the detected intensity contains an interference term involving z_0, which results from the phase difference of the last terms in Eqs. (4.8b) and (4.18). This heterodyne term is the leading fluctuating term in the intensity, and our experimental setup has been designed specifically to examine this term. The effect of varying z_0 is such that when z_0 is small, the radius of the illuminated spot is approximately w_0, and any squeeze mode with a wavelength $\Lambda > w_0$ will generate a scattered field that overlaps with the specular reflection, giving rise to a fluctuation in the detected intensity. When z_0 is large, the radius of the illuminated spot w_f is larger than w_0 according to Eq. (4.2), and only squeeze modes with $\Lambda > w_f$ contribute to fluctuations in the detected intensity. In this case of large z_0, the different phase variations of $\mathbf{E}_{\text{specular}}$ and $\mathbf{E}^{(\mathbf{K})}_{\text{squeeze}}$ over the detector surface lead to the washout of fluctuations in intensity due to modes with $w_0 < \Lambda < w_f$.

This dependence of the detected intensity on the film-waist separation z_0 is illustrated in Fig. 4 and will be explored further after an expression for the detected power is derived in Sec. IV B.

B. Fluctuations in the detected power

The total intensity at a point on the detector is the absolute value squared of the total electric field:

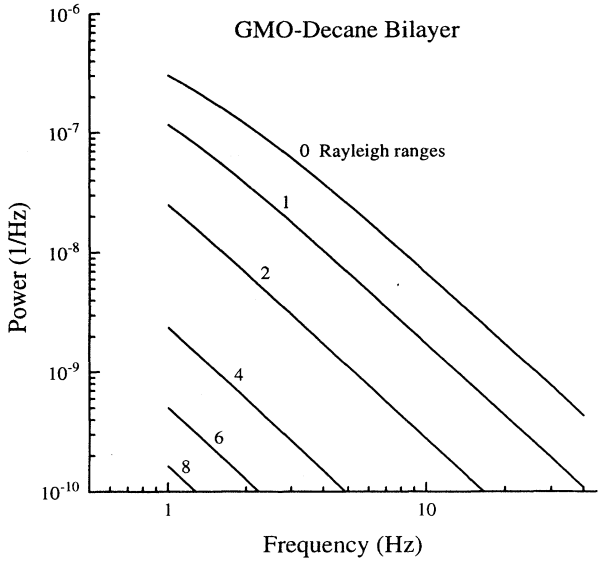

FIG. 4. Predicted RFS spectra for a GMO–decane bilayer when the film-waist distance z_0 is 0, 1, 2, 4, 6, and 8 Rayleigh ranges. The corresponding radii of the illuminated spots on the film are given by Eq. (4.2). In evaluating Eq. (4.26), the following values for parameters were used: thickness compressibility $= U'' = 10^{13}$ J/m^4, film viscosity $= \eta = 7.5 \times 10^{-3}$ Pa sec, interfacial tension $= \sigma = 3.84 \times 10^{-3}$ N/m [22], hydrodynamic thickness of the film $= h_0 = 4.81$ nm [22], optical thickness of film $= h_{\text{op}} = 5.77$ nm [28], refractive index of the film $= n_2 = 1.44$ [28], refractive index of the surrounding water $= n_1 = 1.33$, radius of laser waist (86%) $= w_0 = 3.25$ μm, and laser wavelength $= \lambda_0 = 633$ nm.

$$I_{\text{total}}=|\mathbf{E}_{\text{total}}|^2=|\mathbf{E}_{\text{specular}}+\mathbf{E}_{\text{squeeze}}|^2$$
$$=I_{\text{specular}}+2\text{Re}\{\mathbf{E}^*_{\text{specular}}\cdot\mathbf{E}_{\text{squeeze}}\}+I_{\text{squeeze}} \tag{4.19}$$

where we define

$$\mathbf{E}_{\text{squeeze}}=\sum_{\mathbf{K}}\mathbf{E}^{(\mathbf{K})}_{\text{squeeze}}\ ,\quad I_{\text{specular}}=|\mathbf{E}_{\text{specular}}|^2\ ,$$
$$I_{\text{squeeze}}=|\mathbf{E}_{\text{squeeze}}|^2\ .$$

The amplitudes of the thermally generated squeeze modes fluctuate in time, so the terms involving $\mathbf{E}_{\text{squeeze}}$ in Eq. (4.19) represent fluctuations in the total intensity. The power recorded by the detector is obtained by integrating the intensity over the detector surface:

$$P_{\text{total}}=\int_{A_{\text{det}}}\int dA\ I_{\text{total}}$$
$$=P_{\text{specular}}+2\int_{A_{\text{det}}}\int dA\ \text{Re}\{\mathbf{E}^*_{\text{specular}}\cdot\mathbf{E}_{\text{squeeze}}\}$$
$$+P_{\text{squeeze}}\ . \tag{4.20}$$

The mean-square fluctuation in the total detected power is

$$\langle[P_{\text{total}}-\langle P_{\text{total}}\rangle]^2\rangle=4\left\langle\left[\int_{A_{\text{det}}}\int dA\ \text{Re}\{\mathbf{E}^*_{\text{specular}}\cdot\mathbf{E}_{\text{squeeze}}\}\right]^2\right\rangle+\langle[P_{\text{squeeze}}-\langle P_{\text{squeeze}}\rangle]^2\rangle$$
$$\cong 4\left\langle\left[\int_{A_{\text{det}}}\int dA\ \text{Re}\{\mathbf{E}^*_{\text{specular}}\cdot\mathbf{E}_{\text{squeeze}}\}\right]^2\right\rangle\ , \tag{4.21}$$

where the angular brackets indicate a time average, and we have used the fact that $\Delta h(\mathbf{K},t)$ in Eq. (4.18) is a complex Gaussian random variable with zero mean. In the final form of Eq. (4.21), we have neglected the (homodyne) fluctuations in the squeeze power because $E_{\text{specular}}\gg E_{\text{squeeze}}$, so the heterodyne term dominates.

After the integral over the detector area in Eq. (4.21) is performed and the result is squared, the time average can be used to simplify the expression

$$\langle[P_{\text{total}}-\langle P_{\text{total}}\rangle]^2\rangle=P_0^2 4\frac{(n-1)^2}{(n+1)^2}\sin^2(k_2h_{\text{op}})k_1^2(n^2-1)^2\cos^2k_2h_{\text{op}}\sum_{\mathbf{K}}\langle|\Delta h(\mathbf{K},t)|^2\rangle\{\text{Re}[D(K)]\}^2\ , \tag{4.22}$$

where we have used the statistical independence of thermally excited squeeze modes expressed in Eq. (3.6). In Eq. (4.22), P_0 is the power of the incident beam, and $D(K)$ results from the integral over the detector area,

$$D(K)\equiv w_0^2k_1^2\exp\left[-\tfrac{1}{4}w_0^2K^2\left[1+i\frac{z_0}{z_R}\right]\right]\int_0^{\theta_{\text{det}}}d\theta\sin\theta\exp[-\tfrac{1}{2}w_0^2k_1^2\sin^2\theta]I_0\left[\tfrac{1}{2}w_0^2Kk_1\sin\theta\left[1+i\frac{z_0}{z_R}\right]\right]\ , \tag{4.23}$$

where θ_{det} is the angular radius of the detector, and $I_0(z)$ is the modified Bessel function of order zero $[I_0(z)=J_0(iz)]$.

Experimentally, the angular radius of the detector θ_{det} is set at 7.4°, an ample size to collect the specularly reflected beam whose 99% angular radius is 5.3°. For these small angles, $\sin\theta\approx\theta$ in the integral of Eq. (4.23). Furthermore, $D(K)$ is sufficiently strongly damped in K and θ that the upper limit on the integral may be extended from θ_{det} to infinity without appreciably altering the value of $D(K)$. Then, with the help of integral 6.614.3 in Gradshteyn and Ryzhik [27], $D(K)$ reduces to

$$D(K)=\exp(-\tfrac{1}{8}w_f^2K^2)\ , \tag{4.24}$$

where w_f is defined in Eq. (4.2).

The sum over squeeze wave vectors in Eq. (4.22) can be converted to an integral over wave number according to Eq. (3.7), and the mean-square thickness fluctuation associated with wave vector $\mathbf{K}$ can be evaluated using Eq. (3.8). The frequency spectrum of squeeze modes can be introduced using Eq. (3.9), so that Eq. (4.22) can be rewritten as

$$\langle[P_{\text{total}}-\langle P_{\text{total}}\rangle]^2\rangle=\int_0^\infty d\nu\,P_0^2\frac{16k_BT}{\pi}k_1^2(n-1)^4\sin^2(k_2h_{\text{op}})\cos^2(k_2h_{\text{op}})$$
$$\times\int_0^\infty\frac{K\,dK}{\sigma K^2+2U''}\exp(-\tfrac{1}{4}w_f^2K^2)\frac{\Gamma(K)}{(2\pi\nu)^2+[\Gamma(K)]^2}\ . \tag{4.25}$$

As in Sec. III, we normalize the mean-square fluctuation in detected power by the square of the average power. Since the specular reflection is much stronger than the power scattered by the squeeze modes, the average power detected is given by Eq. (3.11). Finally, we have the following expression for the normalized spectrum of fluctuations in the detected power:

$$S(\nu)=\frac{k_BT}{\pi}k_1^2(n+1)^4\frac{\cos^2(k_2h_{\text{op}})}{\sin^2(k_2h_{\text{op}})}$$
$$\times\int_0^\infty\frac{K\,dK}{\sigma K^2+2U''}\exp(-\tfrac{1}{4}w_f^2K^2)$$
$$\times\frac{\Gamma(K)}{(2\pi\nu)^2+[\Gamma(K)]^2}\ . \tag{4.26}$$

Recall that $\Gamma(K)$ is defined in Eq. (2.1) and w_f is defined in Eq. (4.2).

Notice that Eq. (4.26) is nearly identical to Eq. (3.13), which was derived using a thin-film interference approach. Only the multiplicative constants differ slightly. The discrepancy can be traced to the replacement of the fields in Eqs. (4.4)–(4.6) with the incident field, leading to the approximate form of the multiplicative constant in Eq. (4.26). For a lipid bilayer surrounded by water, Eqs. (3.13) and (4.26) yield values for $S(\nu)$ that are the same to better than 0.4%.

The dependence of $S(\nu)$ on the spot size w_f [or on the film-waist distance z_0 through Eq. (4.2)] is illustrated in Fig. 4 for a GMO–decane bilayer. Notice the sharp reduction in the spectrum as the beam waist is moved off the film. In terms of Sec. III, a larger illuminated spot averages spatially over more squeeze modes, so fewer modes (only those with $\Lambda > w_f$) are able to contribute to fluctuations in the detected intensity. In terms of Sec. IV A, larger values of z_0 lead to more rapid spatial phase fluctuations in the squeeze heterodyne term, and the intensity fluctuations are washed out in the integral over the surface of the detector. In our experimental setup, the Rayleigh range is approximately 52 μm (actually 70 μm in water), so a very small translation of the focusing lens should result in a dramatic decrease in the measured spectrum of intensity fluctuations. This feature provides a simple procedure for discriminating signal from background, especially since the average detected power should remain unchanged.

Another feature to note in Fig. 4 is that a log-log plot of the spectrum of intensity fluctuations versus frequency yields a straight line above a few hertz. For a GMO–decane bilayer, most of the optically important squeeze modes ($\Lambda > 10$ μm) have relaxation rates of less than 5/sec, so that at a few hertz all of the Lorentzians in the integral in Eq. (4.26) exhibit their $1/\nu^2$ wings. The slopes of the spectra in Fig. 4 correspond to this inverse-square power law.

When the laser waist is located on the bilayer ($z_0 = 0$ in Fig. 4), the RFS spectrum deviates from a $1/\nu^2$ dependence at 1 or 2 Hz. The deviation is due to the contributions of squeeze modes with wavelengths in the range of 3 to 10 μm. These modes have Lorentzian widths greater than 1 or 2 Hz, and hence the curvature of the central region of these Lorentzians becomes apparent, as opposed to the $1/\nu^2$ behavior of the wings. As the laser waist is moved off the bilayer and the illuminated spot increases in size, the thickness fluctuations due to these squeeze modes ($\Lambda = 3-10$ μm) are averaged out, and the curvature of the spectrum disappears (e.g., $z_0 = 2$ Rayleigh ranges in Fig. 4). It is important to be able to observe experimentally this low-frequency departure from a $1/\nu^2$ dependence, because only this region allows a determination of the thickness compressibility U''. The $1/\nu^2$ region of the RFS spectrum can yield the film viscosity but is independent of U''.

C. Scattering from the bend mode

On the spatial scale probed by our RFS light-scattering technique (≥ 1 μm), the amplitude of bend motion in a GMO–decane bilayer is 20 times that of thickness fluctuations (see Table I). It is important therefore to determine if scattering from the bend modes will augment or perhaps even overwhelm the squeeze mode contribution [Eq. (4.26)] to the RFS spectrum. The following simple, intuitive line of reasoning suggests that the RFS spectrum is insensitive to bend motion. The detector in our RFS experimental setup records light scattered within a cone of half angle 7.4° centered on the direction of the specular reflection. Because squeeze and bend modes scatter light like gratings, modes that scatter light at small angles must have long wavelengths. Squeeze modes with long wavelengths are experienced by the incident beam as planar films with a time-varying thickness. According to the thin-film interference approach of Sec. 3, this time-varying thickness leads to a time-varying intensity of the specular reflection. In contrast, bend modes with long wavelengths are experienced by the incident beam as planar films moving toward and away from the beam, giving rise to Doppler phase shifts in the reflected electric field. However the *intensity* of the specular reflection is insensitive to these phase shifts, and so the RFS spectrum should be insensitive to scattering by bend modes.

The dynamic light-scattering approach of the present section can be used to quantitatively support this intuitive line of reasoning. Despite the much greater amplitude of bend motion, we shall see that the detected intensity scattered by bend modes is less than that scattered by squeeze modes. Moreover, the power scattered by bend modes is distributed over a spectral width that is five orders of magnitude larger than the spectral width of light scattered from squeeze modes. Hence, light scattered by bend modes contributes insignificantly to the spectrum of fluctuations in detected power over the frequency range 1–100 Hz.

The electric field $\bar{E}^{(\mathbf{K})}_{\text{bend}}(\mathbf{r},t)$ scattered from a bend mode can be calculated with the same procedure used in Sec. IV A to calculate $\mathbf{E}^{(\mathbf{K})}_{\text{squeeze}}(\mathbf{r},t)$. The amplitude $b(\mathbf{K},t)$ of the bend mode with wave vector $\mathbf{K}$ is defined in terms of the associated film displacement $d(\mathbf{r}_f,t)$,

TABLE II. Contributions to the detected power assuming unit power incident upon a GMO–decane bilayer. In calculating the bend power, the longest wavelength of a bend mode was taken to be the bilayer diameter, approximately 1 mm. In calculating the squeeze and bend powers, the angular radius of the detector was taken to be 7.4°. Values of other parameters are given in the caption to Fig. 4.

P_{specular}	P_{squeeze}	$P_{\text{squeeze-heterodyne}} = (P_{\text{specular}} P_{\text{squeeze}})^{1/2}$	P_{bend}
4.29×10^{-5}	6.84×10^{-11}	5.42×10^{-8}	1.56×10^{-8}

$$2d(\mathbf{r}_f,t)=a_{\text{top}}(\mathbf{r}_f,t)+a_{\text{bottom}}(\mathbf{r}_f,t)$$
$$=b(\mathbf{K},t)\exp(i\mathbf{K}\cdot\mathbf{r}_f)\ . \tag{4.27}$$

Two replacements must be made in the results of Sec. IV A,

$$\Delta h(\mathbf{K},t)\rightarrow b(\mathbf{K},t) \quad \text{and} \quad \cos k_2 h_{\text{op}}\rightarrow -i\sin k_2 h_{\text{op}}\ , \tag{4.28}$$

so that the result analogous to Eq. (4.18) for $\mathbf{E}^{(\mathbf{K})}_{\text{squeeze}}(\mathbf{r},t)$ is

$$\mathbf{E}^{(\mathbf{K})}_{\text{bend}}=-\hat{\mathbf{x}}A_0\frac{k_1^2(n^2-1)w_0}{2\sqrt{2\pi}}\Delta b(\mathbf{K},t)\exp[i(k_2-k_1)h_{\text{op}}](-i\sin k_2 h_{\text{op}})$$
$$\times\frac{\exp[i(k_1R_0-\omega t)]}{R_0}\exp(ik_1z_0)\exp\left[-\frac{w_0^2}{4}(\mathbf{K}-\mathbf{q}_f)^2\right]\exp\left[-i\frac{w_0^2}{4}(\mathbf{K}-\mathbf{q}_f)^2\frac{z_0}{z_R}\right]\ . \tag{4.29}$$

The additional factor of $i=\sqrt{-1}$ in the expression for $\mathbf{E}^{(\mathbf{K})}_{\text{bend}}(\mathbf{r},t)$ indicates that the bend field is 90° out of phase with the squeeze field and also with the specularly reflected field [compare Eq. (4.29) with Eq. (4.18) and Eq. (4.8b)]. As a result, the interference (heterodyne) term between E_{bend} and E_{specular} has a time average of zero, so that the leading term in the total intensity due to the bend mode is quadratic in E_{bend} (the homodyne term). Recall that the leading squeeze contribution to the total intensity is a heterodyne term, involving the much larger specularly reflected field and the first power of the squeeze field.

The relative magnitudes of the contributions to the total detected power are summarized in Table II. Equations (4.8), (4.18), and (4.29) were used to calculate the contributions of the specular, squeeze, and bend fields, respectively, for a GMO–decane bilayer. Notice that the leading squeeze term (heterodyne) is 3.5 times larger than the leading bend term (homodyne), even though the amplitude of bend motion is 20 times that of thickness fluctuations.

Consideration of the spectral widths of the squeeze and bend powers finally renders the bend power insignificant. The half width at half maximum (HWHM) of the Lorentzian spectrum due to either a squeeze or bend mode is equal to the relaxation rate Γ [see Eqs. (2.1)–(2.3) and (3.9)]. The relaxation rates for squeeze and bend modes with wavelengths bracketing the important wavelength range are listed in Table III. Notice that the widths of the bend spectra are always about five orders of magnitude greater than those of the squeeze spectra. Because the total powers in the squeeze and bend spectra are roughly the same, the magnitude of the squeeze spectrum in the frequency range used, 1–100 Hz, must be five orders of magnitude greater than that of the bend spectrum.

V. EXPERIMENTAL TEST OF RFS THEORY

As a confirmation of the predictions of Eqs. (3.13) and (4.26), we present typical results of RFS studies of

TABLE III. Relaxation rates (HWHM of RFS spectra) for squeeze and bend modes with wavelengths spanning the range important for RFS measurements. In addition to values listed in the caption to Fig. 4, other parameter values were film density $=\rho=760$ kg/m^3 (51% 1-heptadecene, 49% decane), density of the surrounding water $=\rho'=1000$ kg/m^3, and viscosity of water $=\eta'=0.93\times10^{-3}$ Pa sec.

Λ	ω_{bend} (rad/sec)	Γ_{bend} (1/sec)	Γ_{squeeze} (1/sec)
1 μm	7.6×10^6	2.2×10^7	490
1 mm	910	76	4.9×10^{-4}

GMO–decane bilayers. We have found that these bilayers can be formed reproducibly in water and remain stable for over 24 hours. They contain about 50% decane and are about 5 nm thick. There has been some discussion of thickness fluctuations in GMO–decane bilayers [1], but thus far only our preliminary report [29] has described direct experimental observations of thickness fluctuations. We are now preparing a detailed report of our RFS studies of GMO–decane bilayers and will submit it for publication shortly. Our present abbreviated treatment is intended only to illustrate and substantiate the RFS light-scattering technique.

Although GMO–decane bilayers are attractive in

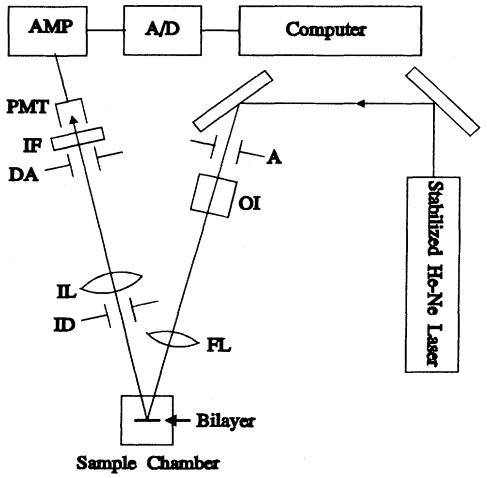

FIG. 5. Schematic of RFS setup. The optics include a Spectra-Physics Model 117A stabilized helium-neon laser, an aperture (A), an optical isolator (OI), a focusing lens (FL) ($f=2$ cm), an iris diaphragm (ID), an imaging lens (IL) ($f=10$ cm), a detector aperture (DA), a 633-nm interference filter (IF), and an EMI Model 9863B/350 photomultiplier tube (PMT) operated at 930 V to achieve a gain of 10 000.

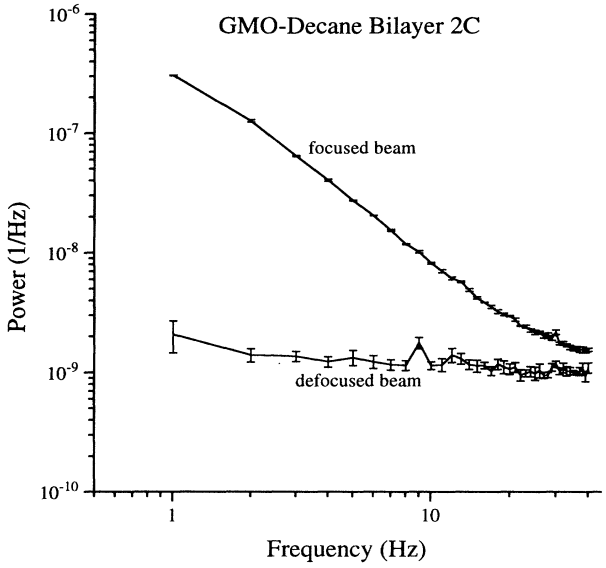

FIG. 6. RFS spectra of a GMO–decane bilayer collected with the laser waist focused on the bilayer (upper curve), and with the waist located 9.5 Rayleigh ranges behind or in front of the bilayer (lower curve). The (focused) waist radius was $w_0 = 3.25$ μm, and the radius of the defocused spot on the bilayer was $w_f = 31$ μm. The solid lines simply connect the data points.

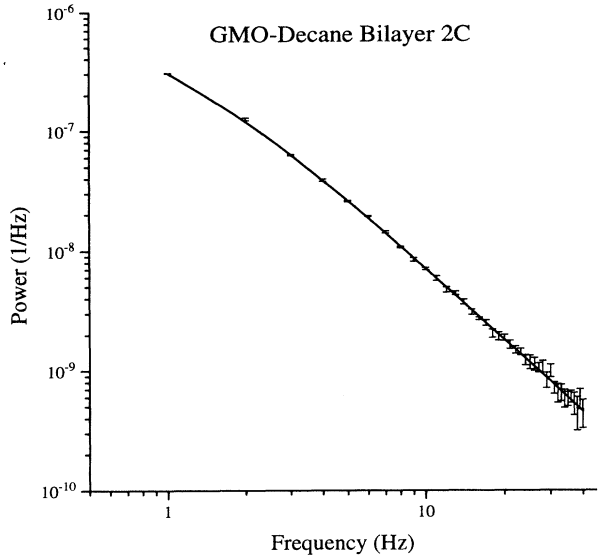

FIG. 7. RFS spectrum of a GMO–decane bilayer after background subtraction. The solid line is a fit to Eq. (3.13) using the film viscosity η and the thickness compressibility U'' as fitting parameters. Values for other parameters (held fixed) can be found in the caption to Fig. 4. The fitted values are $U'' = 10.19(6) \times 10^{12}$ J/m^4, $\eta = 7.07(4)$ mPa sec (cP), and $\chi^2/\nu = 0.77$ ($\nu = 38$).

many ways as a RFS calibration system, they do have some disadvantages. GMO molecules have extensive but not unlimited translational and rotation freedom in the bilayer, leading to an average partial order in orientation of hydrocarbon tails. This anisotropy should affect both molecular dynamics and light scattering. For example, a value for the bilayer viscosity obtained by fitting RFS spectra with our isotropic theory will describe an effective shear motion that is averaged over shear directions contained in the plane of the bilayer and perpendicular to it. Another disadvantage is that the value of the thickness compressibility U'' is not known precisely, and so it is difficult to compare our measured value with a value determined by some independent technique. Nevertheless we do not feel that these drawbacks detract significantly from the remarkable agreement we observe between theory and experiment.

A schematic of our experimental setup is presented in Fig. 5. The beam from a stabilized helium-neon laser is focused onto a bilayer at an angle of 15° from the normal. This small but nonzero angle of incidence can be added to the expression of Eq. (3.13), but the change makes no significant difference. The angular radius of the photodetector is set to a value of 7.4° by an iris diaphragm in the collection optics. A magnified image of the illuminated spot on the bilayer is formed on the detector aperture by an imagining lens. Fluctuations in the photocurrent are recorded and Fourier transformed in real time, and the frequency spectrum of the fluctuations (RFS spectrum) is displayed on a computer monitor.

RFS spectra taken from a representative GMO–decane bilayer are presented in Fig. 6. The focusing lens was translated along the beam axis until the RFS spectrum reached a maximum, indicating the laser waist was positioned on the bilayer. The radius (86%) of the waist was independently measured to be 3.25 ± 0.05 μm. The focusing lens was then translated by 500 μm, which moved the waist 665 μm off the bilayer (9.5 Rayleigh ranges in the water) and increased the radius of the illuminated spot to 31 μm. As illustrated in Fig. 4, this increased spot size should reduce the magnitude of the spectrum drastically. Indeed, the lower curve in Fig. 6 is markedly reduced from the upper, but fundamental photon noise (shot noise) provides a lower limit to fluctuations in the photocurrent. The only way to reduce this background level further is to increase the incident beam power above the 1 mW provided by our Spectra-Physics Model 117A stabilized helium-neon laser.

After subtraction of the photon noise background, the corrected peak spectrum is plotted in Fig. 7. This spectrum has been fitted to the theoretical expression of Eq. (3.13) using the film viscosity η and the thickness compressibility U'' as fitting parameters. The fit is excellent over more than two orders of magnitude. The values of the spectrum at 1, 2, and 3 Hz provide a value for U'' of 10^{13} J/m^4, and a straight-line fit of the ln-ln plot at higher frequencies yields a value for η of 7 mPa sec (centipoise). The value for U'' compares well with the value of 1.2×10^{13} J/m^4 calculated by Hladky and Gruen [1]. Although a thorough discussion of these values will be reserved for a subsequent publication, both values are certainly reasonable.

In summary, we have derived an expression [Eq. (3.13) or (4.26)] for RFS spectra using two different light-scattering approaches (Secs. III and IV). Experimental RFS spectra measured from GMO–decane bilayers are readily fit to the theoretical expression and yield reasonable values for hydrodynamic parameters.

ACKNOWLEDGMENTS

This work was supported by National Science Foundation Grant No. DMB-8603426 to the authors, and by American Chemical Society-Petroleum Research Fund Grant No. 15928-B7 to Dr. Haskell and Grant No. 15927-B7 to Dr. Petersen.

*Present address: Department of Physics and Astronomy, University of Rochester, Rochester, NY 14627.

[1] S. B. Hladky and D. W. R. Gruen, Biophys. J. **38**, 251 (1982).
[2] M. C. Wiener, and S. H. White, Biophys. J. **61**, 434 (1992).
[3] W. Pfeiffer, Th. Henkel, E. Sackmann, W. Knoll, and D. Richter, Europhys. Lett. **8**, 201 (1989).
[4] M. F. Brown, A. A. Ribeiro, and G. D. Williams, Proc. Natl. Acad. Sci. USA **80**, 4325 (1983).
[5] S. B. Hladky and D. A. Haydon, Curr. Top. Membr. Transp. **21**, 327 (1984).
[6] H. W. Huang, Biophys. J. **50**, 1061 (1986).
[7] P. Helfrich and E. Jakobsson, Biophys. J. **57**, 1075 (1990).
[8] H. M. Fijnaut and J. G. H. Joosten, J. Chem. Phys. **69**, 1022 (1978).
[9] A. Vrij, J. G. H. Joosten, and H. M. Fijnaut, in *Advances in Chemical Physics,* edited by I. Prigogine and S. A. Rice (Wiley, New York, 1981), Vol. 48, pp. 329–396.
[10] C. Y. Young, and N. A. Clark, J. Chem. Phys. **74**, 4171 (1981).
[11] E. F. Grabowski and J. A. Cowen, Biophys. J. **18**, 23 (1977).
[12] J. F. Crilly and J. C. Earnshaw, Biophys. J. **41**, 197 (1983).
[13] G. E. Crawford, and J. C. Earnshaw, Biophys. J. **49**, 869 (1986).
[14] J. G. H. Joosten, and H. M. Fijnaut, Chem. Phys. Lett. **60**, 483 (1979).
[15] J. G. H. Joosten, Ber. Bunsenges, Phys. Chem. **88**, 1153 (1984).
[16] G. E. Crawford, and J. C. Earnshaw, Biophys. J. **52**, 87 (1987).
[17] K. Miyakawa, T. Hirakawa, and S. Yamashita, J. Phys. Soc. Jpn. **54**, 445 (1985).
[18] J. Lucassen, M. van den Tempel, A. Vrij, and F. Th. Hesselink, Proc. K. Ned. Akad. Wet. Ser. B **73**, 109 (1970).
[19] A. Vrij, F. Th. Hesselink, J. Lucassen, and M. van den Tempel, Proc. K. Ned. Akad. Wet. Ser. B **73**, 124 (1970).
[20] J. G. H. Joosten, J. Chem. Phys. **80**, 2363 (1984).
[21] J. G. H. Joosten, J. Chem. Phys. **80**, 2383 (1984).
[22] J. Requena, D. F. Billett, and D. A. Haydon, Proc. R. Soc. London Ser. A **347**, 141 (1975).
[23] M. Born, and E. Wolf, *Principles of Optics* (Pergamon, Oxford, 1980), Sec. 1.6.4.
[24] K. S. Schmitz, *An Introduction to Dynamic Light Scattering by Macromolecules* (Academic, New York, 1990).
[25] A. E. Siegman, *An Introduction to Lasers and Masers* (McGraw-Hill, New York, 1971), Chap. 8.
[26] W. J. Duffin, *Electricity and Magnetism* (McGraw-Hill, London, 1980).
[27] I. S. Gradshteyn, and I. M. Ryzhik, *Table of Integrals, Series, and Products* (Academic, New York, 1965).
[28] J. P. Dilger, Biochim. Biophys. Acta **645**, 357 (1981).
[29] R. C. Haskell and D. C. Petersen, Biophys. J. **55**, 111a (1989).